

GHOSTS I: A NEW FAINT VERY ISOLATED DWARF GALAXY AT $D = 12 \pm 2$ MPC

ANTONELA MONACHESI¹, ERIC F. BELL¹, DAVID J. RADBURN-SMITH², ROELOF S. DE JONG³, JEREMY BAILIN⁴, JULIANNE J. DALCANTON², BENNE W. HOLWERDA⁵, H. ALYSON FORD⁶, DAVID STREICH³, MARIJA VLAJIC³, AND DANIEL B. ZUCKER⁷

Accepted version October 8, 2018

ABSTRACT

We report the discovery of a new faint dwarf galaxy, GHOSTS I, using HST/ACS data from one of our GHOSTS (Galaxy Halos, Outer disks, Substructure, Thick disk, and Star clusters) fields. Its detected individual stars populate an approximately one magnitude range of its luminosity function (LF). Using synthetic color-magnitude diagrams (CMDs) to compare with the galaxy's CMD, we find that the colors and magnitudes of GHOSTS I's individual stars are most consistent with being young helium-burning and asymptotic giant branch stars at a distance of $\sim 12 \pm 2$ Mpc. Morphologically, GHOSTS I appears to be actively forming stars, so we tentatively classify it as a dwarf irregular (dIrr) galaxy, although future HST observations deep enough to resolve a larger magnitude range in its LF are required to make a more secure classification. GHOSTS I's absolute magnitude is $M_V \sim -9.85^{+0.40}_{-0.33}$, making it one of the least luminous dIrr galaxies known, and its metallicity is lower than $[\text{Fe}/\text{H}] = -1.5$ dex. The half-light radius of GHOSTS I is 226 ± 38 pc and its ellipticity is 0.47 ± 0.07 , similar to Milky Way and M31 dwarf satellites at comparable luminosity. There are no luminous massive galaxies or galaxy clusters within ~ 4 Mpc from GHOSTS I that could be considered as its host, making it a very isolated dwarf galaxy in the Local Universe.

Subject headings: galaxies: dwarf — galaxies: individual (GHOSTS I)

1. INTRODUCTION

Despite the rapid rate of discovery of new Local Group dwarf galaxies (e.g., Willman et al. 2005; Belokurov et al. 2007; Martin et al. 2009; Slater et al. 2011; Richardson et al. 2011, see McConnachie 2012 for a review), the number of observed dwarf galaxies is far lower than the number of dark matter halos expected around massive galaxies in a cosmological context (e.g., Moore et al. 1999; Klypin et al. 1999). It is widely thought that the most reasonable interpretation of this difference is that most very low mass halos do not host detectable stellar content for a number of possible reasons, including effective feedback from star formation or inefficient gas cooling and accretion (e.g., Dekel & Silk 1986; Bullock et al. 2000; Benson et al. 2002; Koposov et al. 2009). Yet, many modeling uncertainties remain: for example, dramatic variations in galaxy formation efficiency at low mass may be required (Boylan-Kolchin et al. 2012), feedback-driven changes in the central density profile of dwarf galaxies may dramatically reduce the number of surviving Local Group dwarf galaxies (Brooks et al. 2013), and at any rate there is a significant degree of halo-to-halo scatter

expected in dwarf galaxy luminosity functions (Gómez et al. 2012).

One of the interesting open issues is how dwarf galaxies are affected by being close to giant (e.g., Milky Way mass) galaxies. The tidal and ram pressure effects of such a halo are considerable and likely transform many star-forming dwarf irregular [dIrr] galaxies into non-star-forming dwarf spheroidal [dSph] galaxies (e.g., Mayer et al. 2001, 2006). Indeed, it appears quite plausible that even a single pass by a massive galaxy is sufficient to shut off star formation in a dwarf galaxy, leaving a dwarf spheroidal remnant (Slater & Bell 2013; see also Teyssier et al. 2012 and Kazantzidis et al. 2013); such processes can create dSph galaxies out to more than 1 Mpc from the giant galaxy.

Tidal forces strongly affect dwarf galaxies, and those experiencing large tidal forces will get disrupted (e.g., Brooks et al. 2013), leaving an extended stellar halo around massive galaxies (Bullock et al. 2001; Bullock & Johnston 2005; Bell et al. 2008; Cooper et al. 2010). Yet, current surveys are sensitive to ultra-faint $M_V \gtrsim -6.5$ dwarfs only within 300 kpc of the Milky Way (SDSS; Walsh et al. 2009) and M31 (PANDAS; Richardson et al. 2011). Only brighter systems can be seen at larger distances from the Milky Way (e.g., Irwin et al. 2007). Consequently, it is possible that our current dwarf galaxy luminosity functions (e.g., Koposov et al. 2008; Walsh et al. 2009) are incorrect, particularly so at the faint end.

In this context, it is important to make progress towards the long-term goal of characterizing the number and properties of dwarf galaxies very far from giant galaxies. The M81 Group contains ~ 40 dwarf galaxies brighter than $M_I \sim -9$ (Chiboucas et al. 2009, 2013); they all lie within 1.2 Mpc. The Cen A group of galaxies contains ~ 60 dwarfs, with its faintest galaxy having a total magnitude of $M_B \sim -10$ (Karachentsev et al. 2002). The two farthest dwarfs from this group are at ~ 2 Mpc from Cen A and have a total magnitude of $M_B \sim -12$ (Crnojević et al. 2012). Furthermore, most

Electronic address: antonela@umich.edu

¹ Department of Astronomy, University of Michigan, 830 Dennison Bldg., 500 Church St., Ann Arbor, MI 48109, USA

² Department of Astronomy, University of Washington, Seattle, WA 98195, USA

³ Leibniz-Institut für Astrophysik Potsdam, D-14482 Potsdam, Germany

⁴ Department of Physics & Astronomy, University of Alabama, Box 870324, Tuscaloosa, AL 35487, USA

⁵ European Space Agency Research Fellow (ESTEC), Keplerlaan 1, 2200 AG Noordwijk, The Netherlands

⁶ National Radio Astronomy Observatory, P.O. Box 2, Green Bank, WV 24944, USA

⁷ Department of Physics and Astronomy, E7A 317, Macquarie University, NSW 2109, Australia

⁸ Based on observations made with the NASA/ESA Hubble Space Telescope, obtained at the Space Telescope Science Institute, which is operated by the Association of Universities for Research in Astronomy, Inc., under NASA contract NAS 5-26555.

distant dwarf galaxies in both groups, as well as in the Local Group, appear to be star-forming dIrrs, although with some important exceptions (see Pasquali et al. 2005 for a discussion of APPLES 1, a field dwarf spheroidal galaxy at $D = 9$ Mpc not associated with any major cluster of galaxies and Makarov et al. 2012 for a discussion of KKR 25, a dwarf spheroidal galaxy 1.9 Mpc from the Milky Way). In this work, we report on the discovery of a very isolated faint dwarf galaxy (which appears to be a dIrr), projected close to M81 on the sky but at least ~ 6 Mpc more distant than M81 and with a total absolute magnitude of $M_V = -9.85^{+0.40}_{-0.33}$.

2. OBSERVATIONS AND DISCOVERY

The GHOSTS⁹ survey (PI = R. de Jong, HST programs = 10523, 10889, 11613, and 12213) consists of *HST* ACS/WFC and WFC3/UVIS images of various fields in the outskirts of nearby disk galaxies. One of its main goals is to resolve the stars in the halos and thick disks of the sampled galaxies, giving insight into their masses, stellar populations, structures, and degree of substructure. The images are reduced homogeneously through the GHOSTS pipeline (Radburn-Smith et al. 2011, hereafter R-S11). PSF stellar photometry of each image was performed using DOLPHOT (Dolphin 2000) and various diagnostic parameters were used to discriminate spurious detections (mostly contamination from unresolved galaxies) from the actual stars. Several selection criteria to discriminate unresolved galaxies from stars were optimized using deep archival high-redshift HST/ACS fields. These were applied to the raw photometric output, which removed $\sim 95\%$ of the contaminants. We refer the reader to R-S11 for full details of the GHOSTS data pipeline and the photometric culls. The final catalog of stars is largely free of background contaminants.

Visual inspection of the drizzled GHOSTS images revealed a dwarf galaxy candidate, partially resolved into individual stars, in one of the HST/ACS fields located in the halo of M81 (HST program 11613, PI = de Jong, Field 16 in Monachesi et al. 2013). The drizzled HST/ACS image of each *F606W* and *F814W* filter is produced using the STScI Multidrizzle routine¹⁰ after combining only two exposures per filter, and therefore detection and rejection of cosmic rays is challenging. Indeed, there were some obvious cosmic rays left in the images when the default values for the Multidrizzle parameters were used. Since contamination by cosmic rays hamper the detection of individual stars, we performed a more careful cosmic ray rejection in the region around the dwarf by using the pixel-based charge transfer efficiency corrected images and optimizing the parameter values, especially those for creating the median image and the cosmic ray masks that are used by Multidrizzle when combining the images. The new HST/ACS combined images, both in *F606W* and *F814W*, clearly show the dwarf galaxy, GHOSTS I, and the 34 individual stars that can now be resolved. We show in Figure 1 a color HST image of GHOSTS I, in the top panel, and a zoomed-in *F606W*-band HST image with its individual stars indicated by circles in the bottom panel. To estimate the overdensity of stars in the dwarf region, we counted the stars inside 150 randomly-selected areas in the field, covering the same area as the dwarf region¹¹

⁹ GHOSTS=Galaxy Halos, Outer disks, Substructure, Thick disk, and Star clusters

¹⁰ <http://stsdas.stsci.edu/multidrizzle/>

¹¹ Regions near the massive globular cluster discovered in this field

TABLE 1
PROPERTIES OF GHOSTS I

Parameter	Value
α (J2000)	09 ^h 53 ^m 13 ^s .7
δ (J2000)	69° 30' 02" .63
E(B-V) ^a	0.091
D [Mpc]	12 ± 2
M_V	-9.85 ^{+0.40} _{-0.33}
Ellipticity	0.47 ± 0.07
Position angle (N to E)	-39° .43 ± 10°
r_h ["]	3.9 ± 0.3
r_h [pc]	226 ± 38
$(m-M)_0$	30.40 ^{+0.33} _{-0.40}

^a Schlegel et al. (1998).

Figure 2 shows, in the left panel, the color-magnitude diagrams (CMD) of all objects classified as stars by the GHOSTS pipeline for Field 16. Red circles represent the stars spatially coincident with the dwarf. The magnitudes have been corrected for Galactic extinction using the corrected extinction ratios $A_\lambda/E(B-V)$ of 2.47 and 1.53 for *F606W* and *F814W*, respectively, that are to be used with the E(B-V) values from Schlegel et al. (1998) dust maps and an $R_V = 3.1$ extinction law (Schlafly & Finkbeiner 2011). The second to fifth panels, from left to right, show the stars detected inside the dwarf region, for an area of $10'' \times 5''$ (200×100 pixels²) centered at GHOSTS I, and inside three random places in the image covering the same area, respectively. The overdensity of stars around the dwarf galaxy is evident.

After discovering GHOSTS I, we checked the Sloan Digital Sky Survey (SDSS) data to see if it was detected by the survey. We found that GHOSTS I was photometrically identified by SDSS and classified as a galaxy at RA= 09:53:13.75, DEC= +69:30:01.58. There is only information about its integrated photometry and no studies about this galaxy have been done so far.

3. PROPERTIES OF GHOSTS I

To measure the apparent magnitude of GHOSTS I we perform aperture photometry around the galaxy using the IMEX-AMINE/IRAF task. We use an aperture radius of 100 pixels, equivalent to $5''$. We estimate the background contamination by averaging the luminosity of four randomly selected regions across the field, for which we also performed aperture photometry using the same aperture radius. The apparent Galactic extinction-corrected magnitudes of GHOSTS I in Vega-mag *F606W* and *F814W* filters are 20.36 ± 0.2 and 19.73 ± 0.15 , respectively. These magnitudes were converted into $V = 20.60 \pm 0.28$ and $I = 19.54 \pm 0.15$ using the transformations between the HST/ACS and BVRI photometric systems by Sirianni et al. (2005). Its integrated color is $V-I = 1.06 \pm 0.31$. The SDSS integrated colors for this galaxy are $g-r = 0.45 \pm 0.11$ and $g-i = 0.37 \pm 0.15$.

To obtain the galaxy's ellipticity, we fit elliptical isophotes to the dwarf's image using the IRAF task ELLIPSE. The galaxy's ellipticity and position angle were determined from the outer isophotes in the *F814W*-band image. To calculate the dwarf's half-light radius, we fit a Sersic profile function to the surface brightness profiles in both filters, using the isopho-

(Jang et al. 2012) were discarded. We find that the mean number of stars inside the sample of 150 regions is 5 with a standard deviation of $\sigma = 2.25$. Assuming a Poisson distribution in the field of $n=5$ stars per area, the probability of finding 34 stars within the same area is 1.3×10^{-17} .

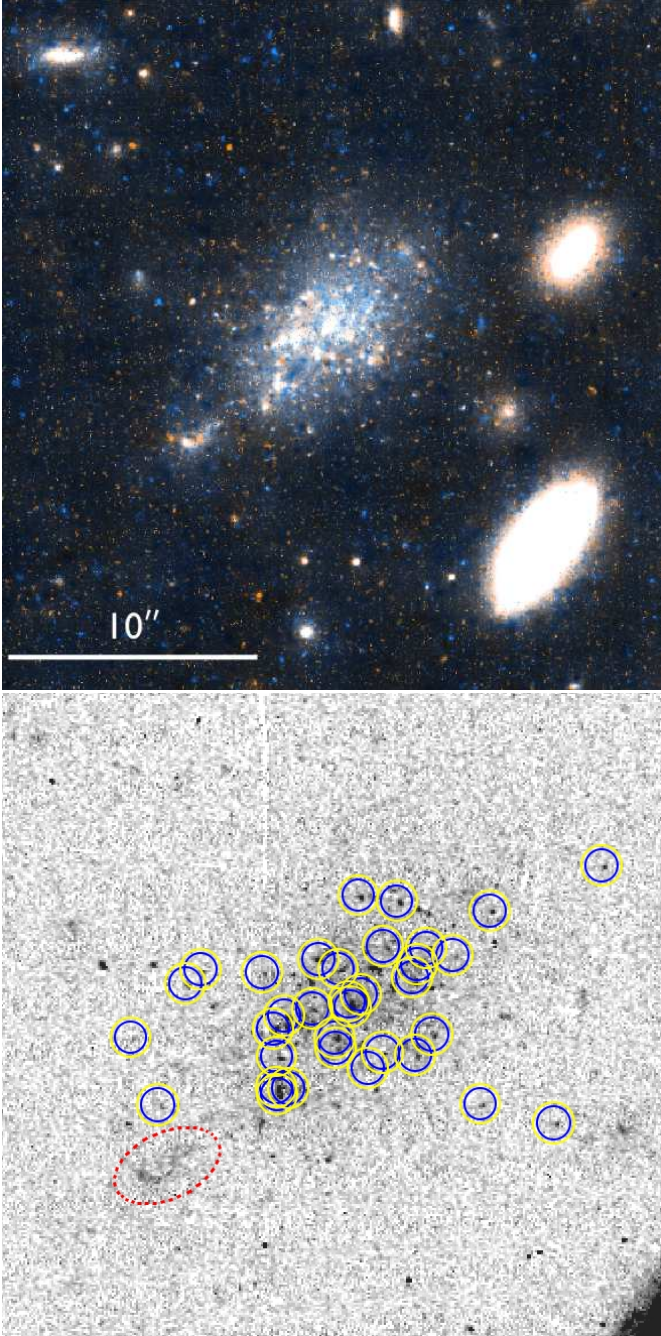


FIG. 1.— HST image of GHOSTS I. Top panel: Color image of GHOSTS I, in one of the GHOSTS fields located at a projected galactocentric distance of 32 kpc from M81, at M81’s distance. The image size is $\sim 24.5'' \times 24.5''$. Bottom panel: Zoom in of the $F606W$ -band image of GHOSTS I, covering an area of $\sim 15''.8 \times 15''.8$. Circles indicate the individual stars in the region of the dwarf detected using the GHOSTS pipeline and the red dashed ellipse indicates a possible star forming region. North is up and east is to the left. Note that some of the 3 circles in the lower left may be deblends of one source.

tal results (see Figure 3). The dwarf’s properties, as well as its sky location, are listed in Table 1.

4. THE DISTANCE OF GHOSTS I

As shown in Fig 2, we only detect approximately a one magnitude range of GHOSTS I’s luminosity function (LF). Since we know neither the distance nor the star formation history (SFH) of the galaxy, the detected stars could be in princi-

ple consistent with different stellar evolutionary phases seen at various distances. In this section, we use model CMDs to evaluate what kinds of stars could be populating the observed LF. The considered models are based on different assumptions of the galaxy’s SFH and they allow us to constrain the dwarf’s distance and therefore its properties, such as its total absolute magnitude and half-light radius.

We use a set of theoretical CMDs with different stellar populations (i.e. different SFHs) generated using the IAC-STAR code (Aparicio & Gallart 2004). Each model CMD covers different ages and metallicities. The total age and metallicity ranges used are 0 to 12 Gyr and $Z= 0.0001$ to 0.0019 , respectively. For each model CMD, we assume various distances in the range of 4 to 18 Mpc. Given a distance, the absolute magnitudes of the model stars are transformed into apparent magnitudes. We then populate each model CMD with randomly extracted mock stars until the cumulative luminosity matches the observed luminosity of GHOSTS I. In other words, we generate model CMDs at different distances that have the same total luminosity as GHOSTS I.

To make a fair comparison between the properties of GHOSTS I’s stars and those from the model CMDs, we simulate the observational effects (incompleteness and photometric errors) on the extracted mock stars using the results obtained from the extensive artificial star tests (ASTs) as follows (see also Monachesi et al. 2012, 2013). Each star in the model CMD is assigned a magnitude and color correction from the AST results. This correction is the difference between the injected and recovered magnitudes of a randomly selected artificial star of similar magnitude and color to the model star. If the randomly selected artificial star is lost (due to crowding or magnitude detection limit), the model star is also considered "lost". Therefore, after the results from the ASTs are simulated, each model CMD is carefully corrected for completeness and photometric errors as a function of both magnitude and color.

As a last step before comparing the observed CMD against models, we need to take into account the foreground contamination of M81 field stars. We have shown in the previous section that M81 field stars overlap in color and magnitude with the dwarf galaxy stars. Using the 150 random field CMDs (see section 2), we have generated an average foreground CMD by calculating the mean number of field stars as a function of magnitudes. The magnitudes and colors assigned to those stars per magnitude bin were calculated using the mean and standard deviation values from all the field stars in that particular magnitude bin. The foreground CMD was added to each model CMD.

Finally, the resulting (model + foreground) CMD is quantitatively compared with the CMD of GHOSTS I to assess the viability of each model and each distance. Specifically, we compare the number of stars as a function of magnitude. For the cases where the number of stars coincides, within Poisson uncertainties, their color distributions are compared. Figure 4 shows the comparison between the LF of GHOSTS I, indicated with a red line, and some of the models (from top to bottom) at different distances (from left to right), indicated with black dashed lines. The errorbars indicate Poisson uncertainty. For the cases where both model and observed LFs agree (letters A, B, C, and D in Figure 4) we compare their color distributions, shown in Figure 5 with the same corresponding letter, and make the final decision as to whether the model and specific distance are acceptable. Figure 6 shows some examples of the model (black dots) and M81 foreground

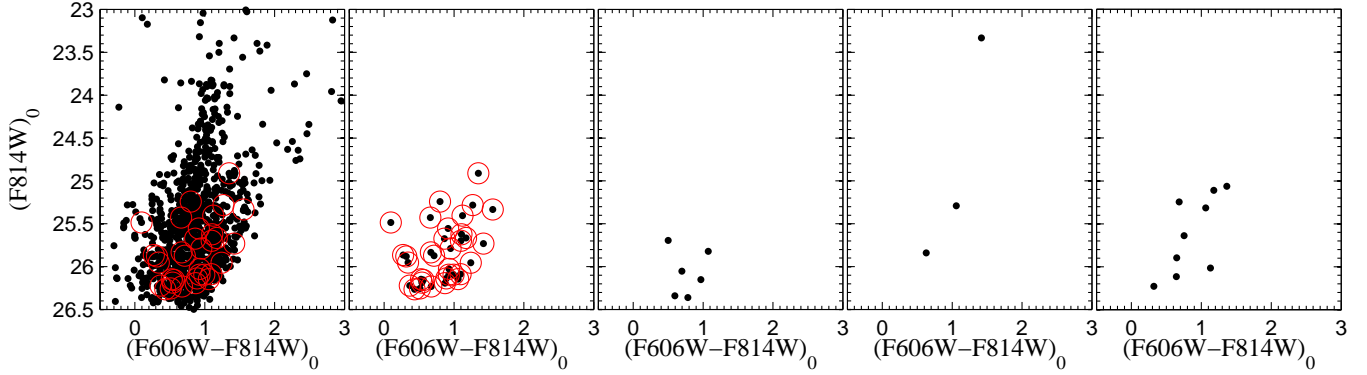


FIG. 2.— First panel: CMD of stars in M81’s halo field with the probable dwarf member stars highlighted with red circles. Second panel: CMD of stars within $10'' \times 5''$ (200×100 pixels 2) centered at the dwarf. Third to fifth panels: CMDs of stars within $10'' \times 5''$ (200×100 pixels 2) around three randomly chosen field locations. There is a clear overdensity of stars where the dwarf is located. More precisely, there are 34 ± 5.8 stars within the dwarf region, where the uncertainty is due to Poisson error, whereas the mean number of stars within a same area of 150 randomly-selected regions in the field is 5 ± 2.25 .

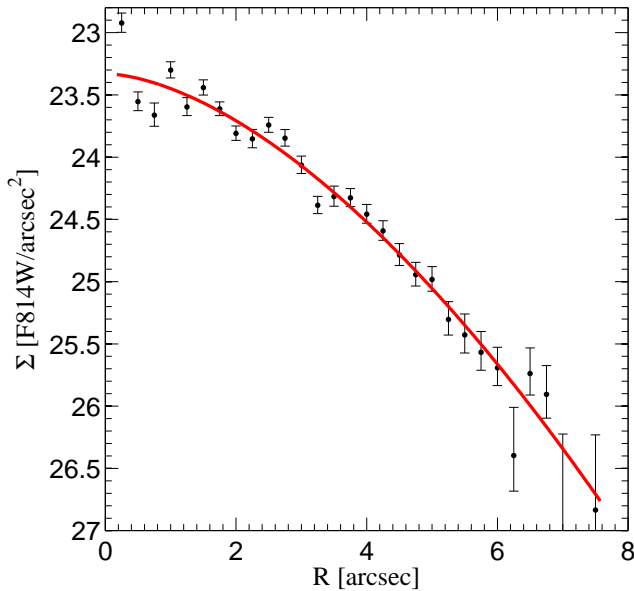


FIG. 3.— $F814W$ -surface brightness profile of GHOSTS I, as obtained by the isophotal fitting. The red curve indicates a Sersic profile fit. The half-light radius and Sersic index obtained from this fit are $r_h = 3''.9 \pm 0''.3$ (or 149 ± 11 pc at the dwarf distance), and $n = 0.6 \pm 0.17$, respectively.

stars (gray dots) CMDs, which are to be compared with the GHOSTS I CMD, shown in each panel as red circles.

From these quantitative comparisons, we find that the most likely distance of GHOSTS I is 12 ± 2 Mpc and that the stars that we observe are very young (0–200 Myr) blue and red helium-burning stars (BHeB and RHeB) as well as young AGB stars. In what follows, we describe and discuss some of the relevant considered scenarios:

- *Faint RGB stars at M81’s distance ($D \sim 3.7$ Mpc):* A first straightforward hypothesis to analyze is that GHOSTS I is a satellite of M81. The dwarf galaxy’s resolved stars could be red giant branch (RGB) stars at the distance of M81, since their apparent magnitudes and colors seem consistent with those of faint RGB stars in the M81’s field CMD (see leftmost panel in Fig 2). From the LFs comparison procedure outlined above, we find that *none* of the models at 4 Mpc, no matter what stellar populations we use, agrees with the

LF of GHOSTS I. If GHOSTS I is at M81’s distance, we should have been able to statistically observe at least 7 RGB stars in the dwarf brighter than $F814W \sim 25$ (see, e.g., left panel in the first row of Figure 4) whereas we observe none. For a mean of 7, a Poisson distribution gives a probability of 9×10^{-4} of observing 0 stars. In addition, a LF of M81 field stars, normalized to GHOSTS I’s LF can be seen in the rightmost panel of the first row in Figure 4 as blue line. The different shape in their luminosity functions indicates that GHOSTS I does not have a similar stellar population, and thus it is not a satellite, of M81. We therefore rule out the possibility that the dwarf is at M81’s distance.

- *Old metal poor TRGB stars:* If we consider the case in which the detected stars are old (12 Gyr) metal poor ($[Fe/H] = -2.25$ dex) RGB stars, the brighter stars that we observe would be the tip of its red giant branch (TRGB) from which we can estimate the distance of the dwarf galaxy. The absolute I magnitude of the TRGB is rather constant ($M_I \simeq -4$) for populations older than ~ 3 Gyr with metallicities lower than $[Fe/H] \sim -0.7$ (Bellazzini et al. 2001). Thus, this evolutionary feature is commonly used for dwarf galaxies to determine their distances. We find that the number of stars that we observe in GHOSTS I as a function of magnitude is consistent with a model of such population at $D = 8$ Mpc (see second from left to right panel from the top panel of Figure 4). However, the color distribution of these stars do not match the one of GHOSTS I (see first panels of Figures 5 and 6). Ages between 10 and 13.5 Gyr show similar results; however higher metallicity CMDs are even redder when compared with the color distribution.
- *Tip of the AGB stars:* We consider the possibility that the observed stars are bright asymptotic giant branch (AGB) stars with ages between 1 and 7 Gyr. The AGB also shows a defined tip in the LF, as seen for example in F8D1 (Dalcanton et al. 2009). As previously explained GHOSTS I appears to be a star forming galaxy. Thus, a bright AGB may very well be present in its CMD. Model CMDs generated with a constant star formation rate (SFR) from 12 to 1–7 Gyr ago contain bright AGB stars (brighter than the TRGB) of ages between 1–7 Gyr. Some of these models, e.g., the one

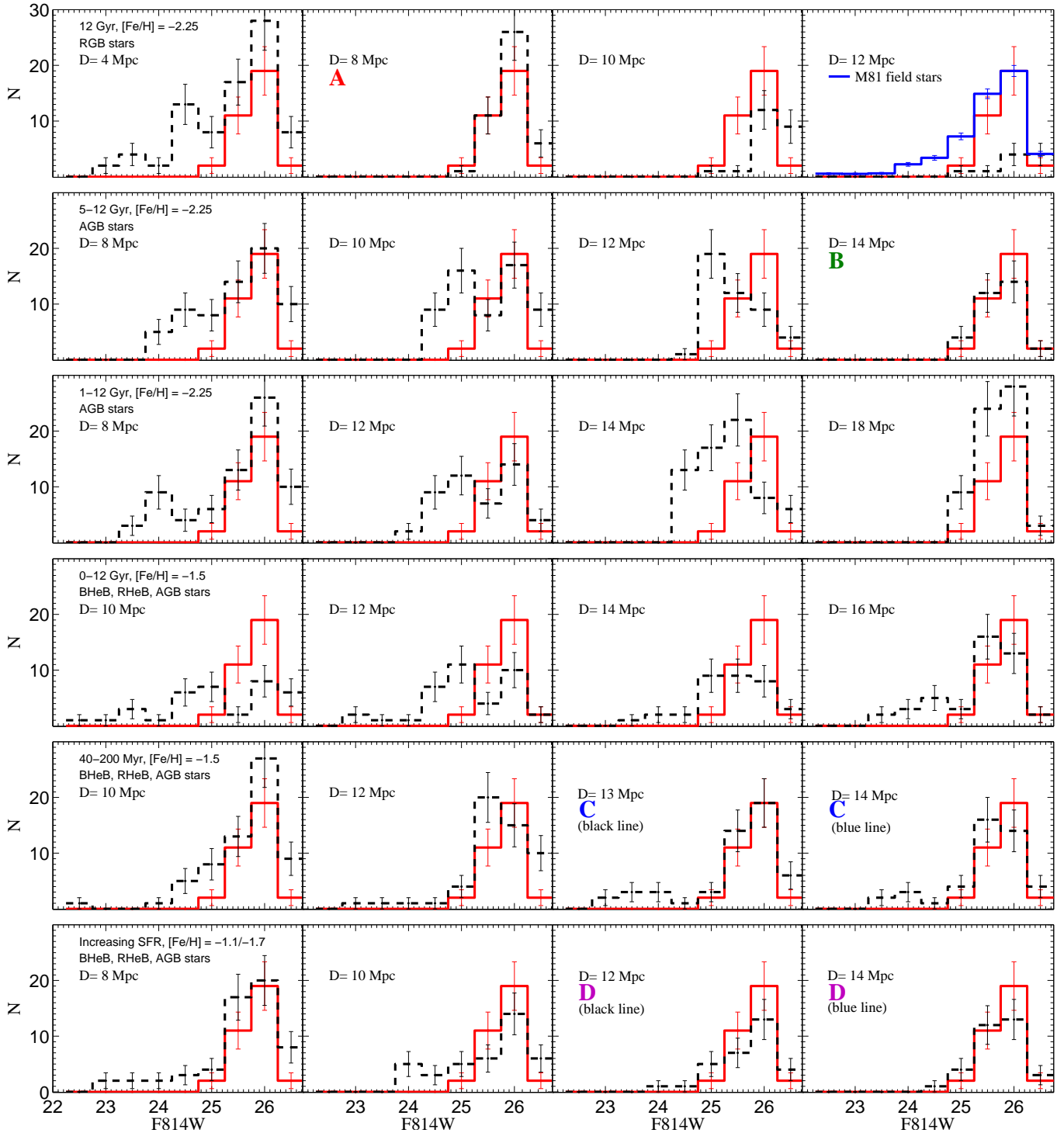


FIG. 4.— Comparison of number of stars as a function of magnitudes between GHOSTS I and different model CMDs that have GHOSTS I’s total apparent magnitude at various distances. Red lines in all panels show the LF of GHOSTS I. Each row indicates a different model CMD, which has been corrected for observational effects and has added an average foreground contamination from M81 field stars. From left to right of each panel we show the resulting model LFs, as black dashed lines, assuming different distances. Errorbars indicate Poisson uncertainties. The panels labeled as *A*, *B*, *C*, and *D* are the ones that match the LF of GHOSTS I and their color distributions are shown in Figure 5 with the same labels. The blue line in the rightmost panel of the first row shows the LF of M81 field stars, scaled to the LF of GHOSTS I. The shape difference between both LFs indicate that GHOSTS I has different stellar populations than M81’s halo and that it is not at M81’s distance. See the text for more details.

with a SFR from 12 to 5 Gyr produce a LF that matches that of GHOSTS I (see second row of Figure 4). However, the mock AGB stars are too red when compared with the observed stars, regardless of the chosen metallicity (see second panel of Figure 5). Figures 4, 5, and 6 show the case in which the most metal poor population available (i.e. having the bluest colors) is considered. We can see from the second panel of figure 6 that the mock bright AGB stars are significantly redder than the data.

- *Young BHeB and RHeB stars:* Another possibility is that the stars that we observe are very young (0–200 Myr) blue and red helium-burning stars (BHeB and RHeB). In particular the RHeB sequence shows well defined tips in the LF, as seen in the dwarf galaxies Holmberg IX and Sextans A (Dalcanton et al. 2009). Morphologically, GHOSTS I looks very clumpy, i.e. not as smooth as a dSph would be. This suggests that GHOSTS I could be actively forming stars and therefore the presence of HeB stars would not be unexpected. We analyzed different models where these kinds of stars are present, e.g. constant SFR from 0 to 12 Gyr ago (see forth row of Figure 4), old stars plus a burst of star formation from 200 to 40 Myr ago (fifth row of Figure 4), and an increased SFR during the last 5 Gyr (last row of Figure 4), for metallicities between $[\text{Fe}/\text{H}] = -1.5$ and $[\text{Fe}/\text{H}] = -2.25$. As shown in Figures 4, 5, and 6, the last two models match nicely both the LF and color distribution of GHOSTS I's stars at distances of 12 ± 2 Mpc. The model with continuous SFR from lookback times of 12 to 0 Gyr did not produce LFs that match the LF of GHOSTS I's stars.

We conclude from this quantitative analysis that the most favorable scenario is the one in which GHOSTS I is a star forming galaxy at $D = 12 \pm 2$ Mpc. Follow up observations of GHOSTS I, in particular deeper HST observations, would help to better constrain the distance to GHOSTS I as well as its stellar population to confirm its nature.

5. DISCUSSION AND CONCLUSIONS

We report the discovery of a faint dwarf galaxy, GHOSTS I, which was detected by visual inspection of one of the HST/ACS GHOSTS fields in the halo of M81. While its integrated light is visible, we resolve individual stars in the dwarf, detecting one magnitude range of its LF. These stars are most likely very young HeB and AGB stars, yielding a distance estimate for GHOSTS I of $\sim 12 \pm 2$ Mpc. Due to its distance and small size on the sky (its half-light radius is $\sim 4''$), the individual stars of GHOSTS I could have not been resolved by a telescope other than HST. In Figure 7 we show the luminosity–size and luminosity–stellar metallicity relations of Local Group and nearby dwarf galaxies (within 3 Mpc; McConnachie 2012). GHOSTS I's derived properties (see Table 1) are typical of nearby dwarf galaxies at its absolute magnitude. Due to the relatively large photometric uncertainties of the star's colors and uncertainties in the isochrone-based metallicities for low metallicities (see Monachesi et al. 2013, Streich et al. 2013), it is difficult to measure the metallicity of GHOSTS I; we expect it to be low ($[\text{Fe}/\text{H}] \lesssim -1.5$) according to the model CMDs that were used in the previous section to compare with the observed CMD.

GHOSTS I is close on the sky to M81 (NGC 3031) with a radial projected distance of only 32 kpc from M81's center,

assuming M81's distance. However, M81's distance is 3.7 Mpc (R-S11), whereas we estimate GHOSTS I's distance to be between 7.9 Mpc and 12.5 Mpc. We searched for giant (luminous and massive) galaxies and clusters of galaxies with heliocentric distance < 16.5 Mpc and within a projected radial distance of 25° from the dwarf's location on the sky, using the updated galaxy catalog by Karachentsev et al. (2013), the distance estimates for 1791 Galaxies from Tully et al. (2008), and NED¹². We found that there are no giant galaxies within 4 Mpc from GHOSTS I. The nearest large galaxy is NGC 3027, at ~ 5 Mpc from the dwarf galaxy, which is one magnitude fainter than M81.

In general, the majority of dwarfs far away from a large galaxy appear to be dIrrs, while those closer to their host galaxies tend to be dSphs. One of the main differences between dIrrs and dSphs is that the latter lack gas and recent star formation, i.e. they stopped forming stars for at least a billion years. On the other hand, dIrrs still retain gas and show evidence of recent star formation, with young stellar populations of ages < 2 Gyr (see review by Tolstoy et al. 2009; McConnachie 2012, and references therein). It has also been noted that dIrrs (within 4 Mpc of the Milky Way) are preferentially found in lower density environments and have higher luminosities at a given size than dSphs (Weisz et al. 2011). The difference in luminosity can be observed in the luminosity-size relation shown in Figure 7, where squares and circles represent dIrrs and dSphs, respectively.

Given their differences in SFHs (Tolstoy et al. 2009; Weisz et al. 2011), the most direct way to distinguish between dIrrs and dSph is to observe or rule out young main sequence (MS) and blue and red helium-burning stars (BHeB and RHeB). GHOSTS I seems to have star forming regions (see red dashed ellipse in Fig. 1), it is morphologically rather clumpy, i.e. not as smooth as a dSph would be, and from the analysis performed in section 4, the most favored explanation for their detected stars is that they are young HeB and AGB stars. Also, from its SDSS color, $g-r = 0.45 \pm 0.11$, it would be considered a star-forming galaxy according to Geha et al. (2012, see their Figure 3), who studied the relative number of quenched versus star-forming dwarf galaxies from SDSS DR8, where quenched galaxies are defined as those which have no $\text{H}\alpha$ emission and a strong 4000 Å break. Furthermore, GHOSTS I is rather isolated (at least ~ 4 Mpc from any giant galaxy), which favors a dIrr, since dSphs are generally found within 1 Mpc from their host galaxy. Thus, we tentatively classify it as a dIrr. Deeper HST images, that could allow us to obtain a CMD detecting at least a 3 magnitude range of GHOSTS I's LF are required to elucidate its true nature. In addition, follow-up spectroscopy of this object will allow us to determine if there are emission lines.

In order to place constraints on the HI content of GHOSTS I, we use the data cube obtained by Chynoweth et al. (2008) using Robert C. Byrd Green Bank Telescope (GBT) observations of a $3^\circ \times 3^\circ$ area centered on the M81 group of galaxies (2003 June 12, Proposal Code = AGBT03B_034_01). Their data cover a very wide velocity range, from -605 to 1970 km s^{-1} , excluding the -85 to 25 km s^{-1} velocity window. Given the distance of GHOSTS I, one expects recession velocities between 700 and 1000 km s^{-1} , depending somewhat on peculiar motions. We find that there is no statistically significant line emission in that velocity range (smoothed to 15 km s^{-1} ,

¹² <http://ned.ipac.caltech.edu/>

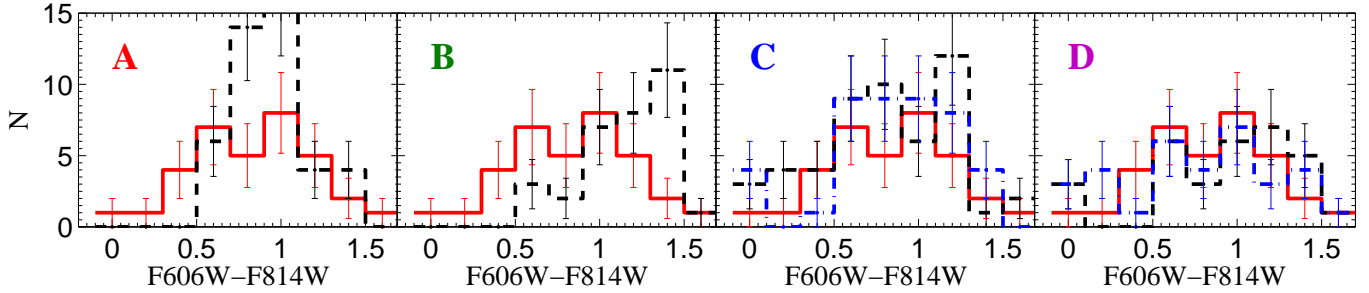


FIG. 5.— Comparing the color distributions of model CMDs with GHOSTS I. The solid red line in each panel indicates the color distribution of GHOSTS I whereas the dashed lines show the color distributions of model CMDs, after the observational effect as well as the foreground M81 field stars contamination were taken into account. All these models have LFs that match the LF of GHOSTS I. The labels in each panel correspond to the labels in Figure 4, i.e. the model in panel *A* is an old metal poor stellar population at 8 Mpc, *B* corresponds to 5–8 Gyr old AGB stars at 14 Mpc, *C* corresponds to a SFH with a burst of star formation between 40 to 200 Myr at 13 and 14 Mpc, and *D* shows the color distribution for a galaxy at 12 and 14 Mpc with an increased SFR during the last 5 Gyr. Clearly, the last two panels match better the color distribution of GHOSTS I.

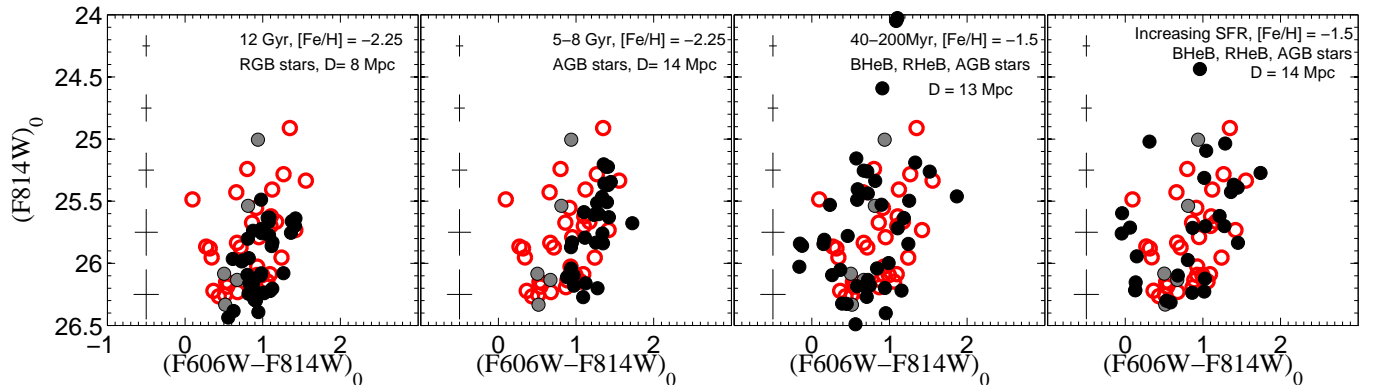


FIG. 6.— Exploring possible scenarios about what kinds of stars populate the one magnitude range of CMD detected in GHOSTS I. In each panel, we show as red circles the stars at the dwarf’s location, as black dots the mock stars after the observational effects were simulated for a galaxy having GHOSTS I’s total apparent magnitude, and as gray dots the average foreground M81 field stars. The errorbars indicate the photometric errors obtained from the ASTs and refer only to color $(F606W - F814W) = 1$. Leftmost panel: The model CMD represents an old, metal poor population at 8 Mpc. The number of stars in the dwarf as well as their magnitudes are consistent with being the brightest portion of the RGB; however their colors distribution differ. Second panel: The brightest stars of this model CMD are AGB stars having ages between 5–8 Gyr at 14 Mpc. We can see that, even though their numbers and magnitudes agree with the stars in the dwarf, their colors are too red. Third panel: Very young HeB and AGB stars populate the one magnitude bright portion of the model CMD at a distance of 13 Mpc. The dwarf’s stars are consistent with being such population. Rightmost panel: The resulting model CMD for a galaxy at $D = 14$ Mpc with increased SFR during the last 5 Gyr. GHOSTS I’s stars are also consistent with being drawn from such a population. See the text for more details.

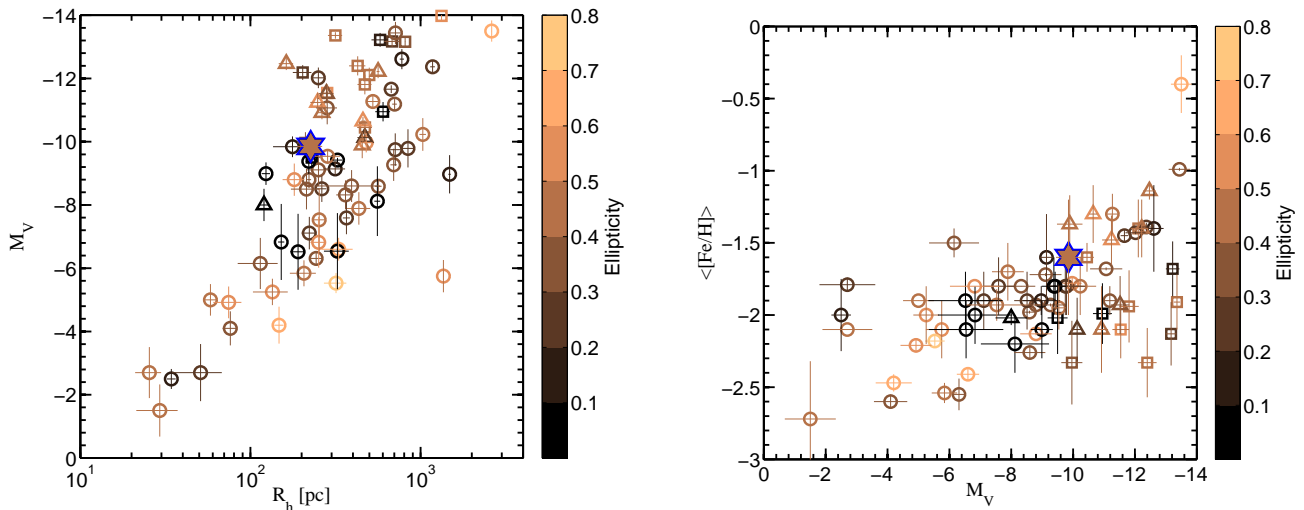


FIG. 7.— Properties of known dwarf galaxies with $M_V > -14$ from data compiled in McConnachie (2012, see references therein). Left panel: Absolute magnitude as a function of size for Local Group and nearby dwarfs within 3 Mpc. The color coding indicates the ellipticity of such objects; black color is used when there was no ellipticity information. dSphs, dIrrs, and transitional type dwarfs (or dwarfs whose dSph/dIrr classification is undetermined) are represented as circles, squares, and triangles, respectively. GHOSTS I is shown as a star. Right panel: stellar metallicity–luminosity relation for dwarf galaxies. Symbols are the same as in the left panel. The properties of GHOSTS I are similar to those of nearby dwarf galaxies at its absolute magnitude.

typical for the velocity width of a dwarf galaxy) at the location of GHOSTS I, placing a 5σ upper limit of its HI mass fraction to $M_{\text{HI}}/L_V < 10.4 M_{\odot}/L_{\odot}$.

If GHOSTS I is indeed a dIrr, it would be, together with Leo P (Rhode et al. 2013) and Leo T (Irwin et al. 2007), one of the faintest and lowest mass star-forming dwarf galaxies. Studying this object will help us understand how these small galaxies retain gas and are able to form stars. If, on the contrary, GHOSTS I is a dSph, it would be the most distant dSph from any large galaxy ever detected, and theoretical models would need to explain how GHOSTS I acquired its morphology without being affected by encounters with a giant galaxy.

AM & EFB are grateful to Mario Mateo for valuable discussions on the different possible stellar populations represented by the dwarf's stars. We thank Katie (Chynoweth) Keating for providing the full M81 group HI data cubes. We wish to thank

the anonymous referee for very useful comments and suggestions that helped to improve this work. This work was supported by HST grant GO-11613, provided by NASA through a grant from the Space Telescope Science Institute, which is operated by the Association of Universities for Research in Astronomy, Inc., under NASA contract NAS5-26555. The National Radio Astronomy Observatory is a facility of the National Science Foundation operated under cooperative agreement by Associated Universities, Inc. This work has made use of the IAC-STAR synthetic CMD computation code which is supported and maintained by the computer division of the Instituto de Astrofísica de Canarias, and also of the NASA/IPAC Extragalactic Database (NED) which is operated by the Jet Propulsion Laboratory, California Institute of Technology, under contract with the National Aeronautics and Space Administration.

Facility: HST (ACS)

REFERENCES

- Aparicio, A., & Gallart, C. 2004, *AJ*, 128, 1465
 Bell, E. F., et al. 2008, *ApJ*, 680, 295
 Bellazzini, M., Ferraro, F. R., & Pancino, E. 2001, *ApJ*, 556, 635
 Belokurov, V., et al. 2007, *ApJ*, 654, 897
 Benson, A. J., Frenk, C. S., Lacey, C. G., Baugh, C. M., & Cole, S. 2002, *MNRAS*, 333, 177
 Boylan-Kolchin, M., Bullock, J. S., & Kaplinghat, M. 2012, *MNRAS*, 422, 1203
 Brooks, A. M., Kuhlen, M., Zolotov, A., & Hooper, D. 2013, *ApJ*, 765, 22
 Bullock, J. S., & Johnston, K. V. 2005, *ApJ*, 635, 931 (B105)
 Bullock, J. S., Kravtsov, A. V., & Weinberg, D. H. 2000, *ApJ*, 539, 517
 —. 2001, *ApJ*, 548, 33
 Chiboucas, K., Jacobs, B. A., Tully, R. B., & Karachentsev, I. D. 2013, *AJ*, 146, 126
 Chiboucas, K., Karachentsev, I. D., & Tully, R. B. 2009, *AJ*, 137, 3009
 Chynoweth, K. M., Langston, G. I., Yun, M. S., Lockman, F. J., Rubin, K. H. R., & Scoles, S. A. 2008, *AJ*, 135, 1983
 Cooper, A. P., et al. 2010, *MNRAS*, 406, 744
 Crnojević, D., Grebel, E. K., & Cole, A. A. 2012, *A&A*, 541, A131
 Dalcanton, J. J., et al. 2009, *ApJS*, 183, 67
 Dekel, A., & Silk, J. 1986, *ApJ*, 303, 39
 Dolphin, A. E. 2000, *PASP*, 112, 1383
 Geha, M., Blanton, M. R., Yan, R., & Tinker, J. L. 2012, *ApJ*, 757, 85
 Gómez, F. A., Coleman-Smith, C. E., O'Shea, B. W., Tumlinson, J., & Wolpert, R. L. 2012, *ApJ*, 760, 112
 Irwin, M. J., et al. 2007, *ApJ*, 656, L13
 Jang, I. S., Lim, S., Park, H. S., & Lee, M. G. 2012, *ApJ*, 751, L19
 Karachentsev, I. D., Makarov, D. I., & Kaisina, E. I. 2013, *AJ*, 145, 101
 Karachentsev, I. D., et al. 2002, *A&A*, 385, 21
 Kazantzidis, S., Łokas, E. L., & Mayer, L. 2013, *ApJ*, 764, L29
 Klypin, A., Kravtsov, A. V., Valenzuela, O., & Prada, F. 1999, *ApJ*, 522, 82
 Kopesov, S., et al. 2008, *ApJ*, 686, 279
 Kopesov, S. E., Yoo, J., Rix, H.-W., Weinberg, D. H., Macciò, A. V., & Escudé, J. M. 2009, *ApJ*, 696, 2179
 Makarov, D., Makarova, L., Sharina, M., Uklein, R., Tikhonov, A., Gubathakurta, P., Kirby, E., & Terekhova, N. 2012, *MNRAS*, 425, 709
 Martin, N. F., et al. 2009, *ApJ*, 705, 758
 Mayer, L., Governato, F., Colpi, M., Moore, B., Quinn, T., Wadsley, J., Stadel, J., & Lake, G. 2001, *ApJ*, 559, 754
 Mayer, L., Mastropietro, C., Wadsley, J., Stadel, J., & Moore, B. 2006, *MNRAS*, 369, 1021
 McConnachie, A. W. 2012, *AJ*, 144, 4
 Monachesi, A., Trager, S. C., Lauer, T. R., Hidalgo, S. L., Freedman, W., Dressler, A., Grillmair, C., & Mighell, K. J. 2012, *ApJ*, 745, 97
 Monachesi, A., et al. 2013, *ApJ*, 766, 106
 Moore, B., Ghigna, S., Governato, F., Lake, G., Quinn, T., Stadel, J., & Tozzi, P. 1999, *ApJ*, 524, L19
 Pasquali, A., Larsen, S., Ferreras, I., Gnedin, O. Y., Malhotra, S., Rhoads, J. E., Pirzkal, N., & Walsh, J. R. 2005, *AJ*, 129, 148
 Radburn-Smith, D. J., et al. 2011, *ApJS*, 195, 18 (RS11)
 Rhode, K. L., et al. 2013, *AJ*, 145, 149
 Richardson, J. C., et al. 2011, *ApJ*, 732, 76
 Schlafly, E. F., & Finkbeiner, D. P. 2011, *ApJ*, 737, 103
 Schlegel, D. J., Finkbeiner, D. P., & Davis, M. 1998, *ApJ*, 500, 525
 Sirianni, M., et al. 2005, *PASP*, 117, 1049
 Slater, C. T., & Bell, E. F. 2013, *ArXiv e-prints*
 Slater, C. T., Bell, E. F., & Martin, N. F. 2011, *ApJ*, 742, L14
 Teyssier, M., Johnston, K. V., & Kuhlen, M. 2012, *MNRAS*, 426, 1808
 Tolstoy, E., Hill, V., & Tosi, M. 2009, *ARA&A*, 47, 371
 Tully, R. B., Shaya, E. J., Karachentsev, I. D., Courtois, H. M., Kocevski, D. D., Rizzi, L., & Peel, A. 2008, *ApJ*, 676, 184
 Walsh, S. M., Willman, B., & Jerjen, H. 2009, *AJ*, 137, 450
 Weisz, D. R., et al. 2011, *ApJ*, 739, 5
 Willman, B., et al. 2005, *ApJ*, 626, L85